© 2014. Published by The Company of Biologists Ltd | Development (2014) 141, 4149-4157 doi:10.1242/dev.110007

RESEARCH ARTICLE

Reciprocal myocardial-endocardial interactions pattern the delay in atrioventricular junction conduction

Michael Bressan‡, PoAn Brian Yang‡, Jonathan D. Louie, Alicia M. Navetta, Robert J. Garriock* and Takashi Mikawa§

ABSTRACT

Efficient blood flow depends on two developmental processes that occur within the atrioventricular junction (AVJ) of the heart: conduction delay, which entrains sequential chamber contraction; and valve formation, which prevents retrograde fluid movement. Defects in either result in severe congenital heart disease; however, little is known about the interplay between these two crucial developmental processes. Here, we show that AVJ conduction delay is locally assigned by the morphogenetic events that initiate valve formation. Our data demonstrate that physical separation from endocardial-derived factors prevents AVJ myocardium from becoming fast conducting. Mechanistically, this physical separation is induced by myocardial-derived factors that support cardiac jelly deposition at the onset of valve formation. These data offer a novel paradigm for conduction patterning, whereby reciprocal myocardial-endocardial interactions coordinate the processes of valve formation with establishment of conduction delay. This, in turn, synchronizes the electrophysiological and structural events necessary for the optimization of blood flow through the developing heart.

KEY WORDS: Action potential, Atrioventricular junction, Conduction velocity diversification, Heart patterning, Optical mapping

INTRODUCTION

Coordinated contraction of the heart requires precise regional patterning of cardiomyocyte conduction velocity. During development, the first cardiac contractions are stimulated by electrical impulses that initiate in the inflow of the primitive heart tube and uniformly propagate towards the outflow (Bressan et al., 2013; Kamino, 1991). This results in a simple peristaltic/suction mechanism for pumping fluids (Forouhar, 2006; Männer et al., 2010). Formation of electrical impulse delay in the atrioventricular junction (AVJ) of the heart represents a key transition in cardiac function. This ensures effective unidirectional blood pumping, as AVJ impulse delay allows for atrial systole to complete prior to the initiation of ventricular contractions. Accordingly, dysfunction in atrial-to-ventricular conduction represents a life-threatening component of several human congenital cardiac syndromes (Clark et al., 2006; Garg et al., 2003; Schott et al., 1998). However, despite more than a century of investigation into the atrioventricular conduction system (Tawara, 1906; Efimov et al., 2004), the mechanisms that restrict slower conduction velocity to this region remain poorly understood.

In parallel with the emergence of conduction delay, paracrine factors from the AVJ myocardium support the formation of the endocardial cushions, which will give rise to the atrioventricular cuspid valves (Butcher and Markwald, 2007; Combs and Yutzey, 2009; Ma et al., 2005; Person et al., 2005; Singh et al., 2012). This process involves swelling of the extracellular matrix (ECM)-rich cardiac jelly within the AVJ. Notably, swelling of the ECM also physically separates the endocardial layer of the heart from the slow-conducting AVJ myocardium, creating a primitive valvular system which prevents retrograde blood flow during the cardiac cycle.

Several endocardial-derived factors have previously been reported to be inducers of fast conduction fate in myocardial cells at later stages of heart development (Gourdie et al., 1998; Hall et al., 2004; Patel and Kos, 2005; Rentschler et al., 2002; Sedmera et al., 2008; Takebayashi-Suzuki et al., 2000). To date, however, it has yet to be examined whether the physical separation of endocardium from myocardium that occurs during cardiac jelly deposition plays a role in AVJ conduction patterning. Current models for how the AVJ becomes slow conducting are focused on the cell-autonomous role of myocardial expressed factors, including *Bmp2*, *Tbx2* and *Tbx3* (Christoffels et al., 2004b; Kokubo et al., 2007; Singh et al., 2005, 2012). It is believed that these factors prevent myocardial differentiation in the AVJ, forcing these cells to retain the slow-conduction characteristics of juvenile myocytes (Christoffels et al., 2004a).

In the present study, the electrophysiological, molecular and morphogenic events that occur concomitant with the heart's transition from a peristaltic pump to a multi-chambered system were examined. Our data demonstrate that the physiological and molecular characteristics of the AVJ myocardium are distinct from juvenile myocytes. Furthermore, both gene expression and impulse propagation can be converted to a fast-conducting phenotype either by implanting AVJ myocytes adjacent to the endocardium of the cushions or through exposure to endocardial-derived paracrine factors. These data indicate that AVJ myocardium must be separated from endocardial-derived factors to become slow conducting, supporting a novel model for how electrical impulse delay is patterned in the AVJ. Accordingly, we propose that AVJ cardiac jelly deposition, which occurs at the initiation of valve formation, alters the local balance of signaling cues supporting slow conduction fate in the AVJ.

RESULTS

AVJ myocytes differentiate with physiological features unique from atrial and ventricular myocytes

To examine how slow conduction is specifically assigned to the AVJ, we mapped changes of physiological and molecular parameters along the entire heart during early chick cardiogenesis from HH stages (st) 10 through 18 (Hamburger and Hamilton, 1951)

Cardiovascular Research Institute, University of California San Francisco, 555 Mission Bay Boulevard South, San Francisco, CA 94143-3120, USA.
*Present address: NIH/NIAID, Bldg 31 Rm A32, 31 Center Drive MSC 2510, Bethesda, MD 20892, USA.
‡These authors contributed equally to this work

§Author for correspondence (takashi.mikawa@ucsf.edu)

Received 11 March 2014; Accepted 27 August 2014

Development (2014) 141, 4149-4157 doi:10.1242/dev.110007

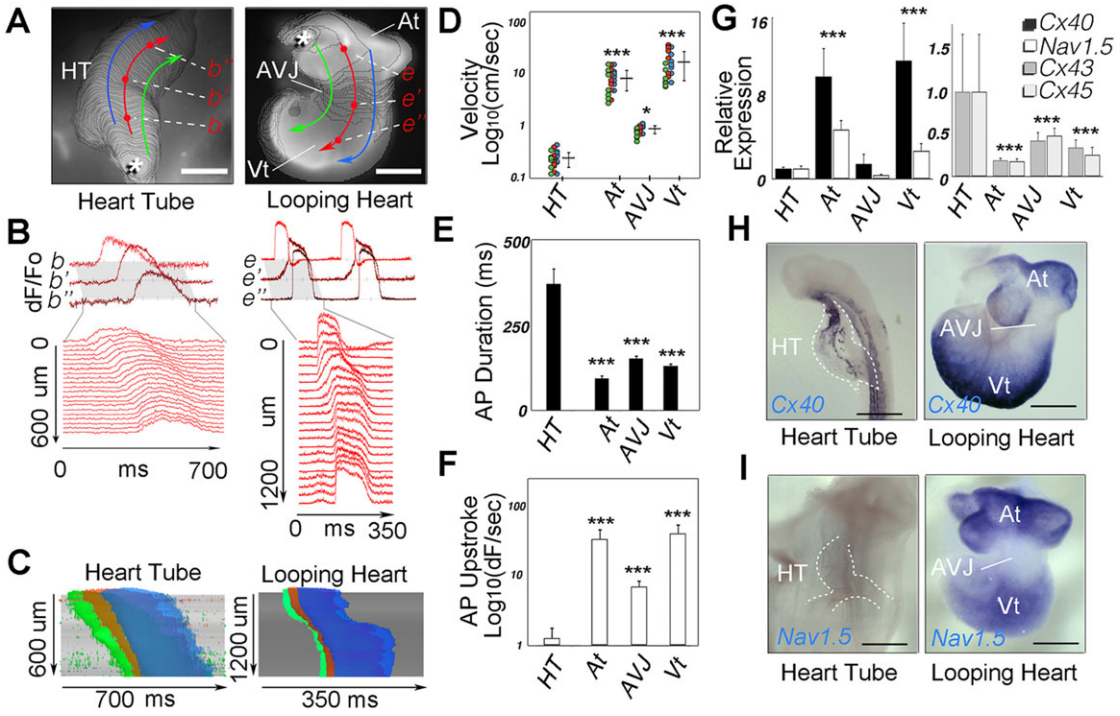

Fig. 1. Regionalization of conduction velocity during cardiac development. (A) Isochronal maps (4 ms/div) demonstrating impulse propagation through a linear heart tube-stage chick heart (~33 h of development) and a looping-stage chick heart (~68 h of development). Asterisks depict action potential initiation sites. Regions of inner (green line), middle (red line) and outer curvature (blue line) were selected for stripe analysis to calculate conduction velocities. Scale bar in heart-tube image: 250 µm; scale bar in looping-heart image: 500 µm. (B) Optical traces of action potential morphology along red lines in A; traces represent change in fluorescence (dF) divided by initial fluorescence (Fo). (C) Stripe analysis depicting action potential propagation along green, red and blue lines in A superimposed. Linear slopes of heart tube-stage action potential propagation indicate uniform conduction velocity. Note that the slope varies across the looping-stage heart, indicating differing conduction velocities. (D) Quantification of conduction velocity along green, red and blue lines from eight heart tube and eight looping-stage hearts. *P<0.05; ***P<0.001 versus heart tube. (E) Quantification of action potential duration from hearts analyzed in D. ***P<0.001 versus heart tube. (F) Quantification of action potential upstroke velocity from hearts analyzed in D. ***P<0.001 versus heart tube. (G) qPCR analysis of gap junction and ion channel expression between heart tube and looping-stage atria, AVJ and ventricle. ***P<0.001 versus heart tube; all bars: mean ± s.d. (H,I) WISH for *Cx40* (H) and for *Nav1.5* (I) in heart tube-stage hearts and looping-stage hearts. Scale bars: 500 µm. Ht, heart tube; At, atria; AVJ, atrioventricular junction; Vt, ventricle.

(Fig. 1). Voltage dye-based optical mapping analysis (Bressan et al., 2013; Efimov, 2004; Kamino, 1991) revealed distinct conduction characteristics between the heart tube primordium at HH st 10, when it began contracting (Patten and Kramer, 1933), and myocardium at heart-looping stages (HH st 18), when the atria and AVJ have become morphologically distinguishable. At linear-tube stages, action potentials initiated in the left posterior inflow segment of the heart and propagated anteriorly towards the outflow with a uniform velocity of 0.23±0.08 cm/s (Fig. 1A-C; supplementary material Movie 1) (Bressan et al., 2013; Kamino, 1991). Conversely, conduction velocity became regionally heterogeneous during heart looping (Fig. 1A-C; supplementary material Movie 1) (de Jong et al., 1992; Bressan et al., 2013). At these stages, action potentials propagated across the presumptive atria at an average rate of 8.2 cm/s, rapidly decelerated to 0.85 cm/s in the AVJ and progressively accelerated to 16.8 cm/s in ventricular myocardium (Fig. 1D).

Both the early heart tube and the looping-stage AVJ displayed conduction velocities slower than the looping-stage atrial and ventricular myocardium. We therefore examined whether the mechanism for AVJ conduction delay was due to this region uniquely maintaining physiological features of primitive heart tube myocardium, as has been previously suggested (Christoffels et al., 2004a). However, detailed analysis of optical mapping data revealed that action potential characteristics of heart tube myocytes and AVJ myocardium differed greatly. AVJ conduction velocity averaged 3.7-fold higher, action potential upstroke velocity was 5.5-fold faster and action potential duration was 2.4-fold shorter in the AVJ compared with the heart tube (Fig. 1D-F). These data indicate that, as heart morphogenesis proceeds, each cardiac region differentiates with specific action potential characteristics and conduction velocities.

To examine the molecular components associated with regionalization of propagation velocity, we profiled the expression of gap junctions and ion channels previously associated with cardiomyocyte conduction velocity. At HH st 10, mRNAs for *GJa1*, *GJa5* and *GJa7*, which encode for cardiac connexin 43 (Cx43), 40 (Cx40) and 45 (Cx45), respectively (Jansen et al., 2010; Teunissen, 2004), were detected at low levels just above background (Fig. 1G). By HH st 18, however, Cx40, the lowest-resistance cardiac gap junction (Kreuzberg et al., 2006), was expressed robustly in atrial and ventricular myocardium, ~6.7- and 7.8-fold higher, respectively, than in AVJ myocytes (Fig. 1G,H). Cx43 and Cx45 expression, however, did not show similar increases in expression between HH st 10 and HH st 18. (Fig. 1G). Similar to Cx40, the ion channel Nav1.5 (encoded by *Scn5a*), which is responsible for the rapid upstroke component of action potentials in fast-conducting myocardium (Remme et al., 2009; Ruan et al., 2009), was differentially expressed during the diversification conduction velocity. Whereas *Nav1.5* mRNA was barely detectable in the heart tube (Fig. 1G,I), at looping-heart stages its expression was robust in the fast-conducting atria and ventricles but 13.8- and 8.0-fold lower, respectively, in the slow-

Development (2014) 141, 4149-4157 doi:10.1242/dev.110007

conducting AVJ. These data suggest that, as regionalization of conduction velocity is patterned during early heart morphogenesis, molecular markers of faster conduction fate, including *Cx40* and *Nav1.5*, become enriched in the atria and ventricles but remain low in the AVJ.

AVJ conduction velocity is increased by exposure to the paracrine signaling factor Et1

Several paracrine factors have been identified as regulators of developmental conduction fate. These include endothelin-1 (Et1) and neuregulin 1 (Nrg1), both of which have been implicated as potential inducers of fast conduction (Gourdie et al., 1998; Hall et al., 2004; Milan et al., 2006; Patel and Kos, 2005; Rentschler et al., 2002; Sedmera et al., 2008; Takebayashi-Suzuki et al., 2000). Conversely, *Bmp2* is highly expressed by the AVJ and is thought to be a negative regulator of *Cx40* and *Nav1.5* expression through its downstream targets Tbx2 and Tbx3 (Christoffels et al., 2004b; Hoogaars et al., 2004; Singh et al., 2012; Yamada et al., 2000; Boukens and Christoffels, 2012; van den Boogaard et al., 2012).

To test whether these factors could influence conduction patterning in the AVJ, looping-stage hearts were isolated and treated with the signaling factors mentioned above. Initially, hearts were treated for 30 min to confirm the activation of downstream signaling effectors in the myocardium (supplementary material Fig. S1). Following this, hearts were treated for 16 h and conduction velocity was analyzed (Fig. 2). Vegf treatment was used as a control for general receptor tyrosine kinase activation. Et1-treated hearts displayed the most prominent increase in AVJ conduction velocity following treatment, with five out of eight hearts displaying a decreased delay between atrial and ventricular activation (Fig. 2A-C; supplementary material Movie 2). Six out of 11 Nrg1-treated hearts exhibited abnormal activation patterns including intermittent AV block (2/11) and ectopic initiation sites (4/11), but AVJ conduction velocity did not differ from control hearts (Fig. 2C; supplementary material Movie 3). Surprisingly, Bmp2 treatment did not result in significant changes in conduction (Fig. 2A-C; supplementary material Movie 4). Similarly, the Bmp signaling antagonist LDN-193189 (Boergermann et al., 2010) did not influence propagation pattern or eliminate AVJ conduction delay (Fig. 2A-C; supplementary material Movie 4). Consistent with the above findings, upregulation of *Cx40* mRNA in the AVJ was detected following Et1 treatment, but was not evident in other experimental groups (Fig. 2D,E). Interestingly, increased Cx40 expression was not coupled to increased *Nav1.5* expression in the AVJ following Et1 treatment (Fig. 2D,E). General myocardial patterning was also preserved following Et1 treatment, as noted by examination of mRNA for *Nkx2.5*, ventricular myosin heavy chain 1 (*Vmhc1*) and atrial myosin heavy chain 1 (*Amhc1*) (supplementary material Fig. S2) (Yutzey et al., 1994). These data demonstrate that the AVJ myocardium is capable of adopting a faster-conducting

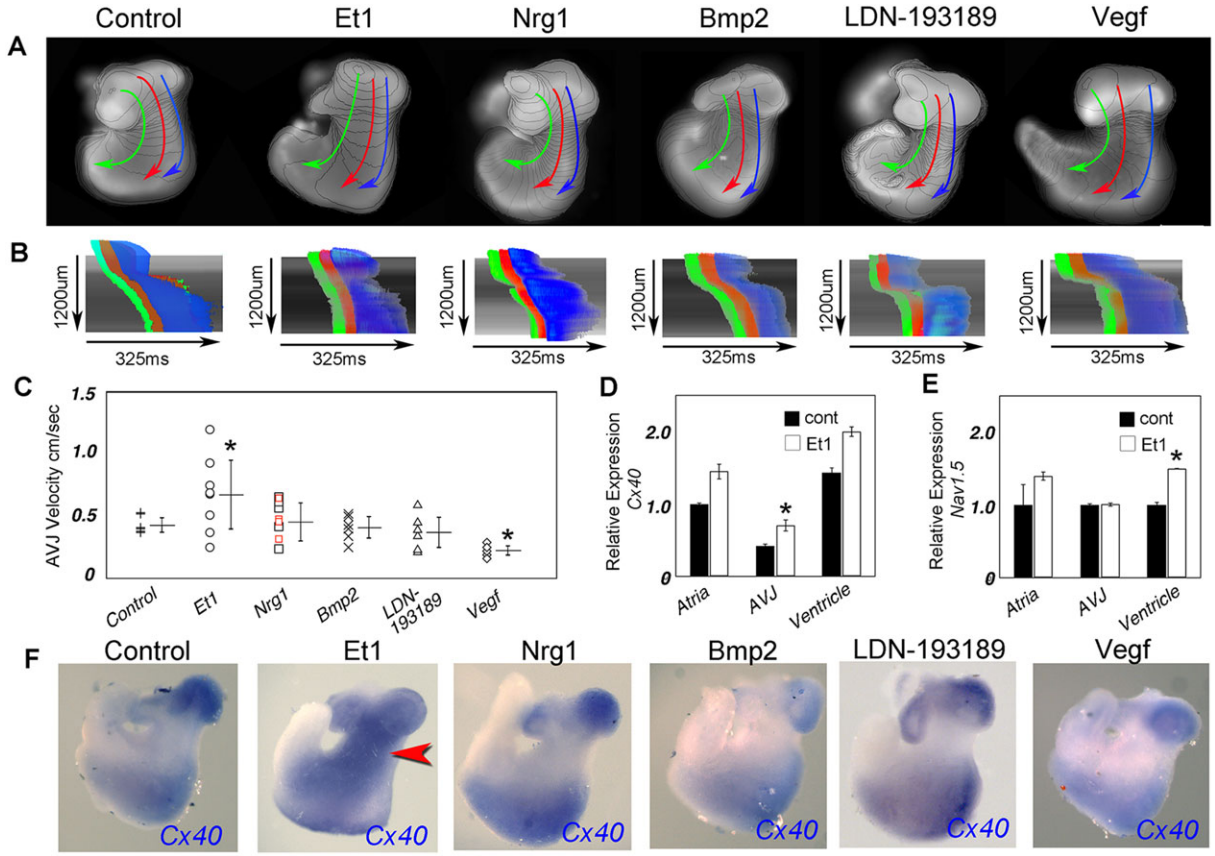

Fig. 2. Et1 increases AVJ conduction velocity. (A) Isochronal maps (4 ms/div) from representative hearts following indicated treatment, Et1 (15 µM), Nrg1 (50 nM), Bmp2 (25 nM), LDN-193189 (1 µM) and Vegf (2.5 µM). Lines along the inner (green), middle (red) and outer curvature (blue) were used for stripe analysis and to calculate average conduction velocity. (B) Stripe analysis of treated hearts from A. (C) Quantification of conduction velocities for treated hearts. Control, *n*=7; Et1, *n*=8; Nrg1, *n*=11; Bmp2, *n*=6; LDN-193189, *n*=7; Vegf, *n*=6. Red data points indicate individual Nrg1-treated hearts with early AVJ activation (see also supplementary material Movie 3). **P*<0.05 versus control. (D,E) qPCR quantification of *Cx40* and *Nav1.5* mRNA following treatment with Et1. **P*<0.05 versus control; all bars: mean ± s.d. (F) Representative WISH for *Cx40* following indicated treatment. Note that Et1 treatment results in ectopic *Cx40* expression in the AVJ (red arrowhead). At, atria; AVJ, atrioventricular junction; Vt, ventricle.

Development (2014) 141, 4149-4157 doi:10.1242/dev.110007

phenotype and can upregulate fast conduction markers such as Cx40 when provided with appropriate paracrine cues.

Proximity to the endocardium defines AVJ conduction velocity

The data shown above indicate that slow conduction is not a developmentally fixed feature of the AVJ and that this region remains capable of responding to inductive cues leading to increased conduction velocity. The ability of Et1 to decrease AVJ conduction delay suggested that lack of availability of endogenous inductive signals might be a contributing factor to how the AVJ escapes fast-conducting fate. To test this model, we examined the expression of endothelin signaling components in looping-stage hearts (HH st 17) (Fig. 3). Whereas endothelin receptor B (*ETbR*) was expressed predominately in the atria and ventricles, endothelin receptor A (*ETaR*) was expressed ubiquitously throughout the myocardium during heart looping (Fig. 3A) (Yanagisawa et al., 1998). Conversely, mRNA for preproEt1, the inactive precursor of Et1, and endothelin-converting enzyme-1 (*Ece-1*) (Masaki, 2004; Yanagisawa et al., 1998), which cleaves the inactive peptide of Et1 to produce the mature Et1 ligand, were absent from the myocardium and restricted to the endocardium in the heart (Fig. 3A,D). Importantly, the swelling of the cardiac jelly within the atrioventricular canal at this stage (Butcher and Markwald, 2007; Combs and Yutzey, 2009; Person et al., 2005) physically separated the endocardium from the myocardium along the AVJ (Fig. 3A,D). This led to the question of whether decreasing the distance between the myocardium and endocardium would be sufficient to increase AVJ conduction velocity.

To test this, the cardiac jelly, a hyaluronic acid-rich ECM between the endocardium and myocardium of the heart, was enzymatically digested *in vivo*. Hyaluronidase (Baldwin and Solursh, 1989; Baldwin et al., 1994; Solursh et al., 1979) was injected directly into the pericardial space of HH st 12 embryos, and these embryos were allowed to develop until HH st 17-18. This broad degradation of hyaluronic acid resulted in morphological defects consistent with those reported in the hearts of hyaluronic synthase 2-knockout embryos (Camenisch et al., 2000). Specifically, treated hearts were enlarged when compared with control embryos (injected with 0.9% saline) (Fig. 4) and lacked uni-directional fluid movement. Alcian Blue staining confirmed that a hyaluronic acid-rich cardiac jelly was absent between the endocardium and myocardium in treated embryos (Fig. 4B,E). Importantly, despite the severe morphological and functional defects in treated hearts, conduction through the AVJ was significantly increased (Fig. 4C,F,G). In control embryos, ventricular activation occurred 82.9±8.3 ms (n=10) after the atria. Conversely, treated embryos displayed a delay of only 51.1±17.7 ms (n=11) (Fig. 4G). The pre-excitation of the ventricle was caused by rapid transmission of action potentials through the dorsal/inferior component of the AVJ. In addition, hyaluronidase-treated embryos displayed ectopic expression of *Cx40* (Fig. 4) and downregulation of *Bmp2* along the dorsal/inferior AVJ, extending from the ventricle to the level at which the AVJ was in contact with the myocardium of the cardiac inflow. These data demonstrate that functional and molecular characteristics of fast-conducting myocardium were induced in the AVJ following ablation of the cardiac jelly. However, as general cardiac morphology in these hearts was perturbed, the specific ability of the endocardium to influence AVJ conduction fate could not be evaluated.

Therefore, to test the ability of the endocardium to influence AVJ fate, we implanted AVJ myocardial cells from HH st 15-16 donor hearts into various regions within the superior endocardial cushion of stage-matched host embryos (Fig. 5). Following an additional

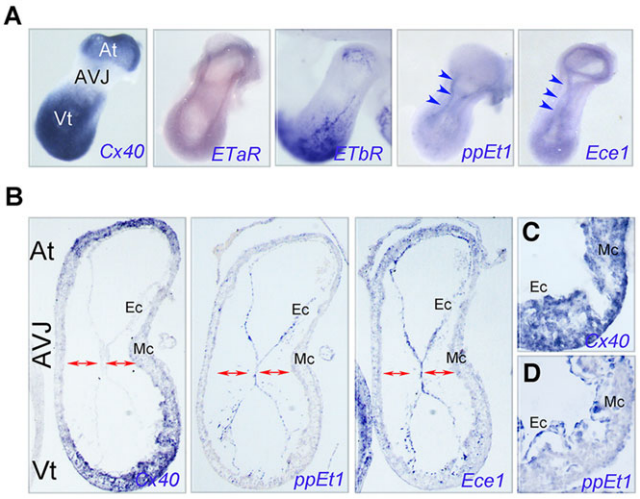

Fig. 3. Endocardial cushions separate source of Et1 from the AVJ myocardium. (A) WISH for *Cx40*, endothelin receptor A (*ETaR*), endothelin receptor B (*ETbR*), *preproEt1* (*ppEt1*) and *Ece1* (left lateral view). (B) Section *in situ* hybridization for *Cx40*, *ppEt1* and *Ece1*. The endocardial cushions separate the ligand and converting enzyme from the *Cx40* negative AVJ (red arrows). (C) Higher magnification image of *Cx40* expression in the ventricular myocardium. (D) Higher magnification image of endocardial *ppEt1*. At, atria; AVJ, atrioventricular junction; Vt, ventricle; Ec, endocardium; Mc AVJ, myocardium.

14 h of incubation the locations and the fates of the implanted cells were examined. Importantly, the overall function and morphology of these hearts was preserved following manipulation. Implanted cells were contracting in the cardiac jelly of host embryos (supplementary material Movie 5), suggesting that these cells were viable, electrically coupled to one another, but electrically isolated from the host heart. The implanted cells expressed *Bmp2*, *Tbx2* and *Tbx3*, at levels comparable to the host AVJ myocytes, thereby also suggesting that the bulk of the implanted tissue did not acquire atrial or ventricular fates following transplantation into the cardiac jelly (Fig. 5G-I). By contrast, the expression of *Cx40* in sister sections showed dramatic changes dependent on the location of implantation (Fig. 5J,K).

Implants that were positioned far from the endocardium expressed *Cx40* at levels similar to the host AVJ myocardium (Fig. 6A,D). Conversely, *Cx40* was upregulated in implants that were near to the host endocardium (Fig. 6B,C,E,F). This trend was further evaluated by quantifying staining intensity in implanted AVJ myocytes as a function of their distance from the endocardium. *Cx40* staining intensity was highest adjacent to the endocardium and tapered as the distance from the endocardium increased (Fig. 6G, n=12). Importantly, this trend was not seen for *Bmp2* staining, which was relatively uniform regardless of distance form the endocardium (Fig. 6H, n=7). These data demonstrate that AVJ myocytes can be induced to express markers of fast conduction *in vivo* and that proximity to the endocardium is a crucial regulator of conduction state.

The above data alone, however, cannot determine whether *Cx40* induction in this system is due to a paracrine interaction with the endocardium, as mechanical deformation of the cardiac jelly during the contraction of the heart could result in stretch-induced activation of *Cx40* (Buschmann et al., 2010) in implanted cells. Therefore, we isolated AVJ myocardial cells as described above and implanted them into mesenchymal populations outside the heart that would not be subjected to the same level of biophysical stretch as in the heart

Development (2014) 141, 4149-4157 doi:10.1242/dev.110007

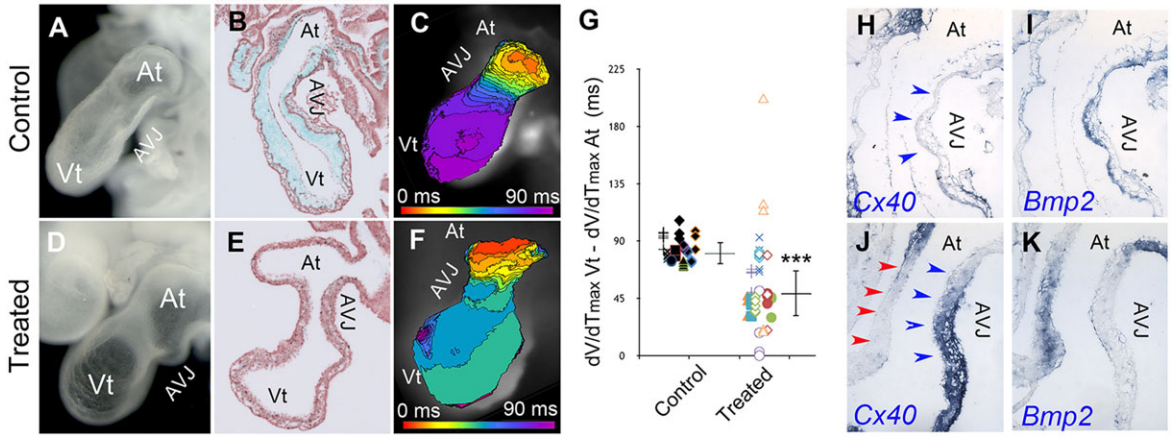

Fig. 4. Digestion of hyaluronic acid leads to remodeling of the AVJ myocardium. (A) Left lateral view of control heart. (B) Sagittal section through control heart stained with Alcian Blue and counterstained with Nuclear Fast Red. (C) Isochronal map of control heart imaged from the left lateral view. (D) Left lateral view of hyaluronidase-treated heart. (E) Sagittal section through hyaluronidase-treated heart stained with Alcian Blue and Nuclear Fast Red. Note the absence of a hyaluronic acid-rich cardiac jelly between endocardium and myocardium. (F) Isochronal map of treated heart imaged from the left lateral view. (G) Quantification of control versus treated atrial to ventricular activation time. Timing of atrial dV/dT_{max} was determined and subtracted from ventricular dV/dT_{max}. Between three and five recordings of each heart were made and data from each control (n=10) and treated heart (n=11) were plotted. ***P<0.001 versus control; bars: average± s.d. (H,I) Higher magnification of AVJ region from B stained for (H) *Cx40* and (I) *Bmp2* mRNA. (J,K) As in H,I, for treated heart in E. *Cx40* expression is upregulated in the dorsal/inferior AVJ (blue arrowheads) compared with the ventral/superior AVJ (red arrowheads), whereas *Bmp2* expression is lost in the dorsal/inferior AVJ.

(Fig. 7). Cells were implanted either into the cranial mesenchyme between the first pharyngeal arch and the midbrain, a region of high endothelin signaling (Clouthier et al., 1998), or the mesenchyme of the limb buds, a region in which high endothelin signaling has not been described. In the limb bud mesenchyme, due to high native expression of *Bmp2*, the cardiac transcription factor *Nkx2.5* was used to identify the site of injected cells in sister sections (Fig. 7K,L). In none of our limb mesenchyme implantations (n=0/4) did we observe induction of *Cx40* mRNA (Fig. 7M). Conversely, within the cranial mesenchyme, robust *Cx40* expression was activated, whereas *Bmp2*, *Tbx2* and *Tbx3* expression were again maintained (Fig. 7F-J, n=5/5). These data confirm that, given the correct inductive environment, *Cx40* expression can be stimulated via stretch-independent paracrine signals. As our above data suggest that proximity to the endocardium is a crucial determinant of whether *Cx40* is expressed, these results demonstrate that proper patterning of the AVJ myocardium requires that these cells be separated from inductive stimuli.

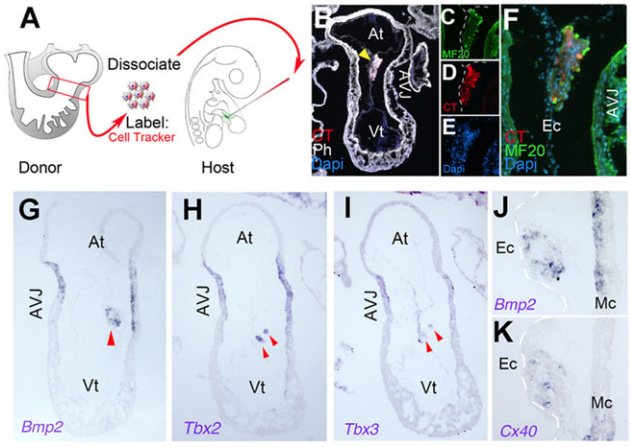

Fig. 5. *In vivo* implantation of AVJ myocytes into host endocardial cushions. (A) Schematic of experimental approach. Donor AVJ myocytes were isolated, dissociated, labeled and microinjected into host superior endocardial cushion (green). (B) Sagittal section through host heart following 14 h of incubation, donor cells are indicated by yellow arrowhead. CT, cell tracker (red), Ph, Phalloidin (white), DAPI (blue). Immunofluorescence for (C) muscle marker MF20, (D) detection of cell tracker and (E) DAPI staining. (F) Merged image of C-E. (G) Section *in situ* hybridization for *Bmp2*. Red arrowhead indicates the position of implanted cells within the host superior endocardial cushion. (H) As in G, for *Tbx2*. (I) As in G, for *Tbx3*. (J) Higher magnification image of implanted cells from G. White dashed line indicates position of the endocardium. (K) Sister section of implant from G,J, stained for *Cx40*. At, atria; AVJ, atrioventricular junction; Vt, ventricle; Ec, endocardium; Mc, myocardium.

DISCUSSION

During heart development, cardiac muscle adopts regional differences in physiological features, including action potential conduction velocity. The upstream events that pattern slow conduction in the AVJ have remained poorly understood. Our data are consistent with a model in which AVJ myocytes are competent to acquire physiological characteristics and a molecular profile indicative of fast-conducting regions of the heart. Furthermore, our data indicate that increased physical distance between AVJ myocytes and endocardial cells is a crucial regulator of conduction velocity, preventing the activation of molecular determinants of faster conduction in AVJ myocytes. As this increased distance is the result of localized swelling of the cardiac jelly at the initiation of valve formation, these findings demonstrate that slowing of conduction velocity between the contractile chambers of the heart and prevention of retrograde blood movement, two crucial processes required for optimization of unidirectional flow, are directly linked during heart development.

When added exogenously to cultured hearts, at least one endocardial-derived factor, Et1, is sufficient to induce faster conduction characteristics in the AVJ. Et1 is thought to be a short-range signaling cue that requires local processing to activate its cognate receptors (Takebayashi-Suzuki et al., 2000; Yanagisawa et al., 1988; Yanagisawa et al., 1998; Yanagisawa, 1994). Consistent with previous studies, our data demonstrate that the transcript for the inactive precursor of Et1, *ppEt1*, is expressed by endocardial cells throughout the heart, as is the membrane-bound metalloproteinase which cleaves and activates Et1, *Ece1* (Masaki, 2004). Additionally, the endothelin receptor, *ETaR*, is expressed throughout the

Development (2014) 141, 4149-4157 doi:10.1242/dev.110007

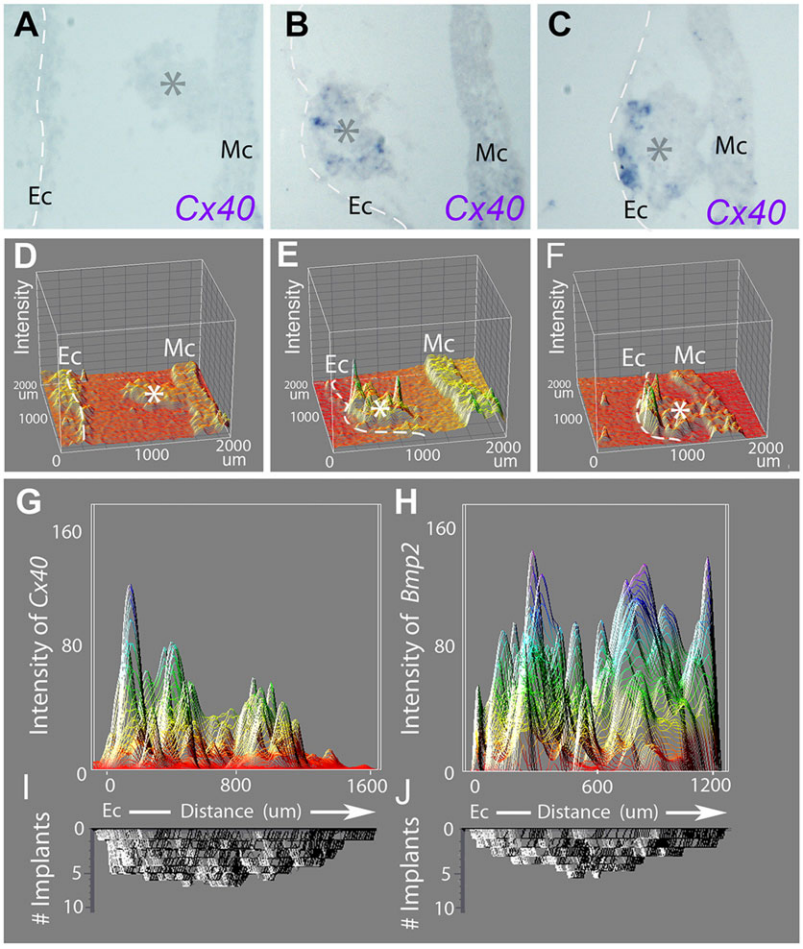

Fig. 6. Proximity to the endocardium regulates *Cx40* expression in AVJ myocytes. (A-C) *In situ* hybridization for *Cx40*. Implanted clusters are indicated by asterisks. (D-F) Intensity plot for *Cx40* staining in A-C. (G) Distribution of maximal staining intensity for *Cx40* relative to distance from the endocardium. This plot was generated by overlaying 12 implants located at varying distances from the endocardium. Intensity units are based on an 8-bit scale (0=minimum possible intensity, 256=maximal possible intensity). (H) As in G, for *Bmp2* (*n*=7). (I) Distribution of implant overlap along the *x*-axis of G. (J) Distribution of implant overlap along the *x*-axis of H.

myocardium during heart looping (Yanagisawa et al., 1998). These qualities make Et1 an attractive candidate factor for the induction of fast conduction phenotypes seen following enzymatic ablation of the cardiac jelly or implantation of AVJ myocytes near the endocardium. However, the current study cannot conclude which factor, or collection of factors, caused AVJ phenotypic conversion in our *in vivo* studies. The identity of the factors responsible and the exact molecular mechanism required for inducing faster conduction characteristics in the AVJ will require further study.

The process of cushion morphogenesis initially depends on the production and secretion of a hyaluronic acid-rich ECM, termed the cardiac jelly, which separates the endocardium from the myocardium along the AVJ. Following this, endocardial cells undergo EMT, invade the jelly and begin the remodeling process that give rise to the valve leaflets. Numerous signaling cascades are involved in these processes (Butcher and Markwald, 2007; Combs and Yutzey, 2009; Craig et al., 2010; Frieden et al., 2010; Garg et al., 2005; Hurlstone et al., 2003; Mercado-Pimentel et al., 2007; Person et al., 2005), with myocardial-expressed factors required for the expression of hyaluronic acid synthase 2, which directly modulates cardiac jelly expansion (Camenisch et al., 2000; Ma et al., 2005; Lagendijk et al., 2011; Shirai et al., 2009; Singh et al., 2012). Our work, therefore, suggests that conduction patterning in the AVJ is the result of a reciprocal myocardial-endocardial interaction, whereby myocardial-derived factors increase the space between the endocardium and myocardium, thus preventing signal reception of endocardial-derived factors in the AVJ myocardium.

This model would predict that modulation of the composition and size of the cardiac jelly would be a crucial component of how AVJ conduction fate is patterned. Indeed, enzymatic ablation of the cardiac jelly results in significant changes in AVJ conduction phenotype, leading to faster propagation through the AVJ. It should be noted, however, that general morphology in the heart was altered dramatically following hyaluronidase treatment, making it difficult to determine the precise interactions responsible for the changes in AVJ conduction.

Therefore, AVJ myocytes were implanted directly into the cardiac jelly of host hearts under conditions in which general cardiac morphology and function were preserved. In these studies, upregulation of the fast conduction marker *Cx40* was observed only in implants that were in close proximity to the endocardium, thus demonstrating that local interaction with the endocardium was sufficient to alter AVJ fate. It should be noted, however, that these findings do not indicate that distance from the endocardium alone is sufficient to prevent fast conduction, as additional positive cues, including those related to biophysical force and hemodynamics, can induce increased conduction velocity and expression of conduction markers in both myocardial and endothelial cells (Buschmann et al., 2010; Zhuang et al., 2000).

Previous studies have demonstrated that intrinsic AVJ characteristics establish slow conduction fate in this region. For instance, it is well-documented that knockout of *Bmp2*, *Tbx2* and *Tbx3* result in ectopic expression of *Cx40* in the AVJ myocardium (Ma et al., 2005; Singh et al., 2012). This is also true when *Bmp2* and *Tbx2* are lost as a result of either *Tbx20* deletion or

Development (2014) 141, 4149-4157 doi:10.1242/dev.110007

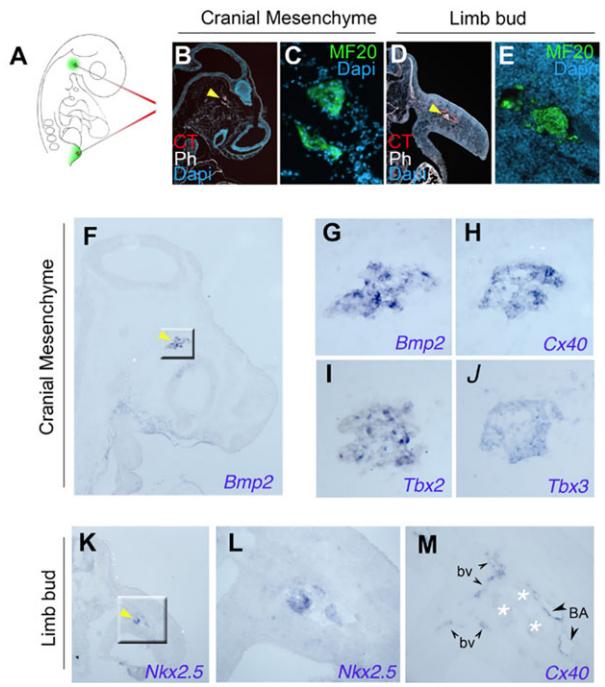

Fig. 7. Local paracrine environment induces *Cx40* in AVJ myocytes. (A) Schematic diagram indicating regions of AVJ-myocyte injections. (B) Location of injected cells (yellow arrowhead) in the cranial mesenchyme 14 h after injection. CT, Cell tracker (red); Ph, Phalloidin (white); DAPI (blue). (C) Higher magnification image of cells from B, stained with the muscle marker MF20 (green). (D,E) As in B,C for limb bud mesenchyme injections. (F) Section *in situ* hybridization for *Bmp2* showing the site of injected AVJ myocytes (yellow arrowhead). (G) Higher magnification image of region outlined in E. (H) Sister section of F,G, stained for *Cx40*. (I) Sister section of F, G, stained for *Tbx2*. (J) Sister section of F,G, stained for *Tbx3*. (K) Section *in situ* hybridization for *Nkx2.5*, indicating location of injected AVJ myocytes (yellow arrowhead) in the host limb bud mesenchyme. (L) Higher magnification image of region from K. (M) Sister section of K,L, stained for *Cx40*. Note that, although the endothelium of limb blood vessels and the brachial artery are positive for *Cx40* (black arrowheads), injected AVJ myocytes are negative (white asterisks).

overexpression of *Hesr1* and *Hesr2* in the myocardium (Kokubo et al., 2007; Singh et al., 2005). Based on *in vitro* studies, ectopic *Cx40* in these knockout models has been attributed to the ability of Tbx2 and Tbx3 to bind and suppress the activity of the *Cx40* promoter. Our data, however, demonstrate that when challenged with positive cues, *Cx40* induction can occur in the AVJ myocardium. It should be noted that neither overexpression nor knockdown techniques were utilized in these studies; therefore, observed responses in our *in vivo* implantation studies were the result of exposure to factors at native physiological levels. As such, this suggests that AVJ myocardium must be separated from positive inductive cues in order to establish a slow-conduction fate. Importantly, this does not preclude the involvement of the Bmp2-Tbx2/3 axis in the patterning of the AVJ cardiac conduction system, but does suggest that additional morphogenetic events are required. Proper patterning of the mature atrioventricular conduction apparatus, including the atrioventricular node and His bundle, is believed to be dependent on a host of transcriptional regulators, including Nkx2.5, Tbx5, Id2 and Gata4 as well as Tbx2 and Tbx3 (Kasahara et al., 2001; Moskowitz et al., 2007; Munshi et al., 2009; Schott et al., 1998). It remains to be determined whether cushion/valve morphogenesis contributes to the later stages of conduction velocity patterning in these structures.

In conclusion, we demonstrate that, given the correct inductive environment, the AVJ myocardium can adopt faster conduction characteristics, and that separation from those inductive cues is required for the AVJ to become slow conducting. This separation is the result of myocardial-derived factors that initiate valve formation. Therefore, the regional patterning of slow-conduction velocity, which is required for the heart to transition from a peristaltic or impedance pump to a multi-chambered system, is not due to a lack of capacity of the AVJ to become fast conducting. Instead, developing myocytes remain plastic, and morphogenetic events separate fast-conducting inductive cues from the myocardium, thereby restricting conduction delay to the AVJ.

MATERIALS AND METHODS

Chicken embryos

Fertilized White Leghorn chicken eggs (*Gallus gallus*) were obtained from Petaluma Farms (Petaluma, CA, USA) and incubated at 38°C until the desired stage. All experiments performed conformed to the University of California animal welfare standards.

Optical mapping of voltage-sensitive dyes

Procedures for optical mapping have been described previously (Bressan et al., 2013). For stripe analysis, regions of interest corresponding to 1 pixel (20 µm) by 60 pixels (1200 µm) were drawn along the inner curvature, middle and outer curvature of hearts. Conduction velocities were calculated as change in distance over change in time along the middle (red) line in each heart. Action potential upstroke velocity was calculated as change in fluorescence (ΔF) over change in time (ΔT) for the period from action potential take off to peak intensity (V_{max}). Action potential duration was calculated as time in milliseconds between 30% V_{max} and 70% repolarization.

Embryonic heart culture

For embryonic heart culture, HH st 17 hearts, including inflow, atria, AVJ, ventricle and three-quarters of the outflow tract, were isolated and transferred to DMEM/F12 media supplemented with 1% penicillin/streptomycin. Hearts were cultured for 30 min for immunohistochemistry or 16 h for physiological and expression analysis at 37°C and 5% CO_2. Et1 (15 µM; Sigma-Aldrich), 50 nM human-recombinant Nrg1 (R&D Systems), 25 nM human-recombinant Bmp2 (R&D Systems), 1 µM LDN-193189 (Stemgent) and 2.5 µM human-recombinant Vegf (Sigma-Aldrich) were added to culture media. These concentrations were chosen based on their ability to elicit activation of downstream signaling in whole-heart cultures (supplementary material Fig. S1). pERk1/2 was used to confirm the activity of Et1 and Nrg1 (Baliga et al., 1999; Clerk et al., 1994), and pSmad1/5/8 was used to confirm the activity of Bmp2 and LDN-193189 (Massague et al., 2005; Boergermann et al., 2010) Endothelin receptor antagonists BQ123 (Sigma-Aldrich) and BQ788 (Sigma-Aldrich) were used at a final concentration of 1 µM.

Hyaluronidase treatment

Hyaluronidase from *Streptomyces hyalurolyticus* (Sigma-Aldrich) was dissolved in a 0.9% saline solution. Between 1 and 2 µl of hyaluronidase at a concentration of 200 U/ml was microinjected into the pericardial space of HH st 12 embryos. Eggs were then sealed and re-incubated for 20 h. During optical mapping of hyaluronidase-treated embryos it was noted that prolonged exposure (longer than 10 min) to the staining solution (Bressan et al., 2013) led to increases in action potential duration and decreased action potential upstroke velocity. Therefore, all recordings analyzed were performed within 5 min of staining.

In vivo implantation of AVJ myocytes

Twenty donor AVJ myocardium explants (HH st 17) were microdissected and pooled, dissociated in 0.05% trypsin for 10 min at 37°C, washed in trypsin-neutralizing solution and then spun down for 8 min at 3000 rpm. Cells were then resuspended in cell tracker 5 µM (Invitrogen) in sterile Tyrode's solution and labeled for 20 min at 37°C. Cells were then spun

Development (2014) 141, 4149-4157 doi:10.1242/dev.110007

down, washed in Tyrode's solution and resuspended in 5 µl of Tyrode's solution. Cells were then backloaded into a silicon-coated glass micropipette (Sigmacote). For injections into the endocardial cushion and cranial mesenchyme host embryos were incubated to HH st 15-16, windowed and cells were pressure-injected into the targeted regions (see Figs 5 and 7). For injections into the forelimbs, host embryos were incubated until HH st 18-19 and cells were injected into the right limb bud. Eggs were then sealed and re-incubated for an additional 14 h. The implanted cells were photo-documented; embryos were then fixed in 4% paraformaldehyde for 45 min and processed for cryosectioning or paraffin embedding.

Whole-mount and section *in situ* hybridization

Whole-mount *in situ* hybridization (WISH) has been described previously (Bressan et al., 2013, Ishii et al., 2010). Probes for *Cx40*, *Nkx2.5*, *AMHC1*, *VMHC1*, *Bmp2*, *Bmp10*, *Tbx2*, *ppEt1*, *Ece1* and *ETbR* have previously been described (Bressan et al., 2013; Hall et al., 2004; Ishii et al., 2010; Takebayashi-Suzuki et al., 2000). Chick *Tbx3*, *ETaR* and *Scn5a* (Nav1.5) were sub-cloned into the pCR II vector (Invitrogen), and Dig-labeled RNA probes were generated.

For quantification of *in situ* hybridization intensity, enzyme-mediated colormetric development of *Cx40* and *Bmp2* probes were carried out for 24 h. Sections were then photographed with and without phase contrast. The intensity of individual implants was evaluated using non-phase contrast images. The geometric center of each cluster was calculated using a weighted area approach. Circles were used to approximate the entire area of the implanted cluster and the center of mass was calculated using Eqn. 1. The shortest distance between the center of mass and the endocardium (defined as the continuous endothelial lining of the heart lumen) was then determined using ImageJ (v10.2). This point was designated as (0,0), and a line was drawn from (0,0) through the center of mass of the implanted cluster. For color intensity measurements, images without phase contrast were used. To control for differences in staining efficiency all images were normalized to host AVJ staining. Based on the above measurements, images of implants were then digitally overlaid in Photoshop using (0,0) and the line transecting the center of mass for alignment. To determine the distribution of maximal staining intensity, the 'darker color' function in Photoshop was used to overlay images. The distribution of maximum intensity was examined as opposed to the sum of intensity to avoid biasing data towards areas of increase implant overlap. The overlaid image was converted to 8-bit greyscale and inverted. The intensity profile of this image was then plotted using ImageJ. In addition to the procedure described above, each implanted cluster was converted into a solid vector mask. These masks were overlaid and the sum of intensities was used to calculate the number of implants overlapping at each region of the intensity plot.

$$\text{Center of mass} = \frac{A_1X_1 + A_2X_2}{A_1 + A_2} \quad (1)$$

Where A_1 and A_2 are the areas of two regions within the implant, and X_1 and X_2 are the distance from the center of these regions to the edge of a line bisecting areas 1 and 2.

Real-time PCR (qPCR)

Tissue was excised from the heart tube or from looping-stage atria, AVJ or ventricles (see supplementary material Fig. S2B). RNA was isolated using RNAeasy kits (Qiagen), and cDNA was synthesized using iScript Select (Bio-Rad) with oligo(dT)s, according to the manufacturer's instructions. Real-time quantitative PCR (qPCR) was performed on a Step-One Plus thermocycler (Applied Biosystems). For qPCR analysis presented in Fig. 1G, in which expression was compared across different stages of development, a combination of Gapdh, α-Tubulin, γ-Tubulin and NKX2.5 were used for normalization with Step One Software (Applied Biosystems v2.1). All other qPCR data comparing expression within the same stage used Gapdh for normalization.

Acknowledgements

We would like to thank Dr Lisa Hua for her help and technical expertise and Dr Sara Venters for her careful reading of the manuscript. A part of this work was included in P.B.Y.'s master's thesis.

Competing interests

The authors declare no competing financial interests.

Author contributions

Scientific approaches for the manuscript were developed by M.B., R.J.G., P.B.Y. and T.M. Experiments were performed by M.B., P.B.Y., J.D.L. and A.M.N. Data analysis was conducted by M.B., P.B.Y., J.D.L., A.M.N., R.J.G. and T.M. The manuscript was prepared and edited by M.B., P.B.Y., J.D.L. and T.M.

Funding

This work was supported in part by grants from the National Institutes of Health [1K99HL122360 to M.B.; T32 HD 007470 to P.B.Y.; and R01 HL093566, R01 HL112268 and R01 HL078921 to T.M.]. Deposited in PMC for release after 12 months.

Supplementary material

Supplementary material available online at
http://dev.biologists.org/lookup/suppl/doi:10.1242/dev.110007/-/DC1

References

Baldwin, H. S. and Solursh, M. (1989). Degradation of hyaluronic acid does not prevent looping of the mammalian heart *in situ*. *Dev. Biol.* **136**, 555-559.

Baldwin, H. S., Lloyd, T. R. and Solursh, M. (1994). Hyaluronate degradation affects ventricular function of the early post looped embryonic rat heart in situ. *Circ Res.* **74**, 244-252.

Baliga, R. R., Pimental, D. R., Zhao, Y. Y., Simmons, W. W., Marchionni, M. A., Sawyer, D. B. and Kelly, R. A. (1999). NRG-1-induced cardiomyocyte hypertrophy. Role of PI-3-kinase, p70(S6K), and MEK-MAPK-RSK. *Am. J. Physiol.* **277**, H2026-H2037.

Boergermann, J. H., Kopf, J., Yu, P. B. and Knaus, P. (2010). Dorsomorphin and LDN-193189 inhibit BMP-mediated Smad, p38 and Akt signalling in C2C12 cells. *Int. J. Biochem. Cell Biol.* **42**, 1802-1807.

Boukens, B. J. and Christoffels, V. M. (2012). Electrophysiological patterning of the heart. *Pediatr. Cardiol.* **33**, 900-906.

Bressan, M., Liu, G. and Mikawa, T. (2013). Early mesodermal cues assign avian cardiac pacemaker fate potential in a tertiary heart field. *Science* **340**, 744-748.

Buschmann, I., Pries, A., Styp-Rekowska, B., Hillmeister, P., Loufrani, L., Henrion, D., Shi, Y., Duelsner, A., Hoefer, I., Gatzke, N. et al. (2010). Pulsatile shear and Gja5 modulate arterial identity and remodeling events during flow-driven arteriogenesis. *Development* **137**, 2187-2196.

Butcher, J. T. and Markwald, R. R. (2007). Valvulogenesis: the moving target. *Philos. Trans. R. Soc. B Biol. Sci.* **362**, 1489-1503.

Camenisch, T. D., Spicer, A. P., Brehm-Gibson, T., Briesterfeldt, J., Augustine, M. L., Calabro, A., Kuback, S., Klewer, S. E. and McDonald, J. A. (2000). Disruption of hyaluronan synthase-2 abrogates normal cardiac morphogenesis and hyaluronan-mediated transformation of epithelium to mesenchyme. *J. Clin. Invest.* **106**, 349-360.

Christoffels, V. M., Burch, J. B. E. and Moorman, A. F. M. (2004a). Architectural plan for the heart: early patterning and delineation of the chambers and the nodes. *Trends Cardiovasc. Med.* **14**, 301-307.

Christoffels, V. M., Hoogaars, W. M. H., Tessari, A., Clout, D. E. W., Moorman, A. F. M. and Campione, M. (2004b). T-box transcription factor Tbx2 represses differentiation and formation of the cardiac chambers. *Dev. Dyn.* **229**, 763-770.

Clark, K. L., Yutzey, K. E. and Benson, D. W. (2006). Transcription factors and congenital heart defects. *Annu. Rev. Physiol.* **68**, 97-121.

Clerk, A., Bogoyevitch, M. A., Anderson, M. B. and Sugden, P. H. (1994). Differential activation of protein kinase C isoforms by endothelin-1 and phenylephrine and subsequent stimulation of p42 and p44 mitogen-activated protein kinases in ventricular myocytes cultured from neonatal rat hearts. *J. Biol. Chem.* **269**, 32848-32857.

Clouthier, D. E., Hosoda, K., Richardson, J. A., Williams, S. C., Yanagisawa, H., Kuwaki, T., Kumada, M., Hammer, R. E. and Yanagisawa, M. (1998). Cranial and cardiac neural crest defects in endothelin-A receptor-deficient mice. *Development* **125**, 813-824.

Combs, M. D. and Yutzey, K. E. (2009). Heart valve development: regulatory networks in development and disease. *Circ. Res.* **105**, 408-421.

Craig, E. A., Austin, A. F., Vaillancourt, R. R., Barnett, J. V. and Camenisch, T. D. (2010). TGFβ2-mediated production of hyaluronan is important for the induction of epicardial cell differentiation and invasion. *Exp. Cell Res.* **316**, 3397-3405.

de Jong, F., Opthof, T., Wilde, A. A., Janse, M. J., Charles, R., Lamers, W. H. and Moorman, A. F. (1992). Persisting zones of slow impulse conduction in developing chicken hearts. *Circ. Res.* **71**, 240-250.

Efimov, I. R. (2004). Optical imaging of the heart. *Circ. Res.* **95**, 21-33.

Efimov, I. R., Nikolski, V. P., Rothenberg, F., Greener, I. D., Li, J., Dobrzynski, H. and Boyett, M. (2004). Structure-function relationship in the AV junction. *Anat. Rec.* **280A**, 952-965.

Forouhar, A. S. (2006). The embryonic vertebrate heart tube is a dynamic suction pump. *Science* **312**, 751-753.

Frieden, L. A., Townsend, T. A., Vaught, D. B., DeLaughter, D. M., Hwang, Y., Barnett, J. V. and Chen, J. (2010). Regulation of heart valve morphogenesis by Eph receptor ligand, ephrin-A1. *Dev. Dyn.* **239**, 3226-3234.
Garg, V., Kathiriya, I. S., Barnes, R., Schluterman, M. K., King, I. N., Butler, C. A., Rothrock, C. R., Eapen, R. S., Hirayama-Yamada, K., Joo, K. et al. (2003). GATA4 mutations cause human congenital heart defects and reveal an interaction with TBX5. *Nature* **424**, 443-447.
Garg, V., Muth, A. N., Ransom, J. F., Schluterman, M. K., Barnes, R., King, I. N., Grossfeld, P. D. and Srivastava, D. (2005). Mutations in NOTCH1 cause aortic valve disease. *Nature* **437**, 270-274.
Gourdie, R. G., Wei, Y., Kim, D., Klatt, S. C. and Mikawa, T. (1998). Endothelin-induced conversion of embryonic heart muscle cells into impulse-conducting Purkinje fibers. *Proc. Natl. Acad. Sci. USA* **95**, 6815-6818.
Hall, C. E. Hurtado, R., Hewett, K. W., Shulimovich, M., Poma, C. P., Reckova, M., Justus, C., Pennisi, D. J., Tobita, K., Sedmera, D. et al. (2004). Hemodynamic-dependent patterning of endothelin converting enzyme 1 expression and differentiation of impulse-conducting Purkinje fibers in the embryonic heart. *Development* **131**, 581-592.
Hamburger, V. and Hamilton, H. L. (1951). A series of normal stages in the development of the chick embryo. *J. Morphol.* **88**, 49-92.
Hoogaars, W. M. H., Tessari, A., Moorman, A. F. M., de Boer, P. A. J., Hagoort, J., Soufan, A. T., Campione, M. and Christoffels, V. M. (2004). The transcriptional repressor Tbx3 delineates the developing central conduction system of the heart. *Cardiovasc. Res.* **62**, 489-499.
Hurlstone, A. F. L., Haramis, A.-P. G., Wienholds, E., Begthel, H., Korving, J., van Eeden, F., Cuppen, E., Zivkovic, D., Plasterk, R. H. A. and Clevers, H. (2003). The Wnt/beta-catenin pathway regulates cardiac valve formation. *Nature* **425**, 633-637.
Ishii, Y., Garriock, R. J., Navetta, A. M., Coughlin, L. E. and Mikawa, T. (2010). BMP signals promote proepicardial protrusion necessary for recruitment of coronary vessel and epicardial progenitors to the heart. *Dev. Cell* **19**, 307-316.
Jansen, J. A., van Veen, T. A. B., de Bakker, J. M. T. and van Rijen, H. V. M. (2010). Cardiac connexins and impulse propagation. *J. Mol. Cell. Cardiol.* **48**, 76-82.
Kamino, K. (1991). Optical approaches to ontogeny of electrical activity and related functional organization during early heart development. *Physiol. Rev.* **71**, 53-91.
Kasahara, H., Wakimoto, H., Liu, M., Maguire, C. T., Converso, K. L., Shioi, T., Huang, W.-Y., Manning, W. J., Paul, D., Lawitts, J. et al. (2001). Progressive atrioventricular conduction defects and heart failure in mice expressing a mutant Csx/Nkx2.5 homeoprotein. *J. Clin. Invest.* **108**, 189-201.
Kokubo, H., Tomita-Miyagawa, S., Hamada, Y. and Saga, Y. (2007). Hesr1 and Hesr2 regulate atrioventricular boundary formation in the developing heart through the repression of Tbx2. *Development* **134**, 747-755.
Kreuzberg, M. M., Willecke, K. and Bukauskas, F. F. (2006). Connexin-mediated cardiac impulse propagation: connexin 30.2 slows atrioventricular conduction in mouse heart. *Trends Cardiovasc. Med.* **16**, 266-272.
Lagendijk, A. K., Goumans, M. J., Burkhard, S. B. and Bakkers, J. (2011). MicroRNA-23 restricts cardiac valve formation by inhibiting *Has2* and extracellular hyaluronic acid production. *Circ. Res.* **109**, 649-657.
Ma, L., Lu, M.-F., Schwartz, R. J. and Martin, J. F. (2005). Bmp2 is essential for cardiac cushion epithelial-mesenchymal transition and myocardial patterning. *Development* **132**, 5601-5611.
Männer, J., Wessel, A. and Yelbuz, T. M. (2010). How does the tubular embryonic heart work? Looking for the physical mechanism generating unidirectional blood flow in the valveless embryonic heart tube. *Dev. Dyn.* **239**, 1035-1046.
Masaki, T. (2004). Historical review: endothelin. *Trends Pharmacol. Sci.* **25**, 219-224.
Massagué, J., Seoane, J. and Wotton, D. (2005). Smad transcription factors. *Genes Dev.* **19**, 2783-2810.
Mercado-Pimentel, M. E., Hubbard, A. D. and Runyan, R. B. (2007). Endoglin and Alk5 regulate epithelial-mesenchymal transformation during cardiac valve formation. *Dev. Biol.* **304**, 420-432.
Milan, D. J., Giokas, A. C., Serluca, F. C., Peterson, R. T. and MacRea, C. A. (2006). Notch1b and neuregulin are required for specification of central cardiac conduction tissue. *Development* **133**, 1125-1132.
Moskowitz, I. P. G., Kim, J. B., Moore, M. L., Wolf, C. M., Peterson, M. A., Shendure, J., Nobrega, M. A., Yokota, Y., Berul, C., Izumo, S. et al. (2007). A molecular pathway including Id2, Tbx5, and Nkx2-5 required for cardiac conduction system development. *Cell* **129**, 1365-1376.
Munshi, N. V., McAnally, J., Bezprozvannaya, S., Berry, J. M., Richardson, J. A., Hill, J. A. and Olson, E. N. (2009). Cx30.2 enhancer analysis identifies Gata4 as a novel regulator of atrioventricular delay. *Development* **136**, 2665-2674.
Patel, R. and Kos, L. (2005). Endothelin-1 and Neuregulin-1 convert embryonic cardiomyocytes into cells of the conduction system in the mouse. *Dev. Dyn.* **233**, 20-28.
Patten, B. M. and Kramer, T. C. (1933). The initiation of contraction in the embryonic chick heart. *Am. J. Anat.* **53**, 349-375.
Person, A. D., Klewer, S. E. and Runyan, R. B. (2005). Cell biology of cardiac cushion development. *Int. Rev. Cytol.* **243**, 287-335.
Remme, C. A., Verkerk, A. O., Hoogaars, W. M. H., Aanhaanen, W. T. J., Scicluna, B. P., Annink, C., den Hoff, M. J. B., Wilde, A. A. M., Veen, T. A. B., Veldkamp, M. W. et al. (2009). The cardiac sodium channel displays differential distribution in the conduction system and transmural heterogeneity in the murine ventricular myocardium. *Basic Res. Cardiol.* **104**, 511-522.
Rentschler, S., Zander, J., Meyers, K., France, D., Levine, R., Porter, G., Rivkees, S. A., Morely, G. E. and Fishman, G. I. (2002). Neuregulin-1 promotes formation of the murine cardiac conduction system. *Proc. Natl. Acad. Sci. USA* **99**, 10464-10469.
Ruan, Y., Liu, N. and Priori, S. G. (2009). Sodium channel mutations and arrhythmias. *Nat. Rev. Cardiol.* **6**, 337-348.
Schott, J.-J., Benson, D. W., Basson, C. T., Pease, W., Silberbach, G. M., Moak, J. P., Maron, B. J., Seidman, C. E. and Seidman, J. G. (1998). Congenital heart disease caused by mutations in the transcription factor NKX2-5. *Science* **281**, 108-111.
Sedmera, D., Harris, B. S., Grant, E., Zhang, N., Jourdan, J., Kurkova, D. and Gourdie, R. G. (2008). Cardiac expression patterns of endothelin-converting enzyme (ECE): implications for conduction system development. *Dev. Dyn.* **237**, 1746-1753.
Shirai, M., Imanaka-Yoshida, K., Schneider, M. D., Schwartz, R. J. and Morisaki, T. (2009). T-box 2, a mediator of Bmp-Smad signaling, induced hyaluronan synthase 2 and Tgfbeta2 expression and endocardial cushion formation. *Proc. Natl. Acad. Sci. USA* **106**, 18604-18609.
Singh, M. K., Christoffels, V. M., Dias, J. M., Trowe, M.-O., Petry, M., Schuster-Gossler, K., Bürger, A., Ericson, J. and Krispert, A. (2005). Tbx20 is essential for cardiac chamber differentiation and repression of Tbx2. *Development* **132**, 2697-2707.
Singh, R., Hoogaars, W. M., Barnett, P., Grieskamp, T., Rana, M. S., Buermans, H., Farin, H. F., Petry, M., Heallen, T., Martin, J. F. et al. (2012). Tbx2 and Tbx3 induce atrioventricular myocardial development and endocardial cushion formation. *Cell. Mol. Life Sci.* **69**, 1377-1389.
Solursh, M., Fisher, M., Meier, S. and Singley, C. (1979). The role of extracellular matrix in the formation of the sclerotome. *J. Embryol. Exp. Morph.* **54**, 75-98.
Takebayashi-Suzuki, K., Yanagisawa, M., Gourdie, R. G., Kanzawa, N. and Mikawa, T. (2000). In vivo induction of cardiac Purkinje fiber differentiation by coexpression of preproendothelin-1 and endothelin converting enzyme-1. *Development* **127**, 3523-3532.
Tawara, S. (1906). *Das Reizleitungssystem des Säugetierherzens*. Jena: Gustav Fischer Verlag.
Teunissen, B. (2004). Transcriptional control of myocardial connexins. *Cardiovasc. Res.* **62**, 246-255.
van den Boogaard, M., Wong, L. Y. E., Tessadori, F., Bakker, M. L., Dreizehnter, L. K., Wakker, V., Bezzina, C. R., 't Hoen, P. A. C., Bakkers, J., Barnett, P. et al. (2012). Genetic variation in T-box binding element functionally affects SCN5A/SCN10A enhancer. *J. Clin. Invest.* **122**, 2519-2530.
Yamada, M., Revelli, J.-P., Eichele, G., Barron, M. and Schwartz, R. J. (2000). Expression of chick Tbx-2, Tbx-3, and Tbx-5 genes during early heart development: evidence for BMP2 induction of Tbx2. *Dev. Biol.* **228**, 95-105.
Yanagisawa, M. (1994). The endothelin system. A new target for therapeutic intervention. *Circulation* **89**, 1320-1322.
Yanagisawa, M., Kurihara, H., Kimura, S., Tomobe, Y., Kobayashi, M., Mitsui, Y., Yazaki, Y., Goto, K. and Masaki, T. (1988). A novel potent vasoconstrictor peptide produced by vascular endothelial cells. *Nature* **332**, 411-415.
Yanagisawa, H., Yanagisawa, M., Kapur, R. P., Richardson, J. A., Williams, S. C., Clouthier, D. E., de Wit, D., Emoto, N. and Hammer, R. E. (1998). Dual genetic pathways of endothelin-mediated intercellular signaling revealed by targeted disruption of endothelin converting enzyme-1 gene. *Development* **125**, 825-836.
Yutzey, K. E., Rhee, J. T. and Bader, D. (1994). Expression of the atrial-specific myosin heavy chain AMHC1 and the establishment of anteroposterior polarity in the developing chicken heart. *Development* **120**, 871-883.
Zhuang, J., Yamada, K. A., Staffitz, J. and Kleber, A. G. (2000). Pulsatile stretch remodels cell-to-cell communication in cultured myocytes. *Circ. Res.* **87**, 316-322.